Eur. Phys. J. Plus (2015) **130**: 194
DOI 10.1140/epjp/i2015-15194-1

THE EUROPEAN PHYSICAL JOURNAL PLUS

Regular Article

Stability analysis of titanium alloy milling by multiscale entropy and Hurst exponent

Rafał Rusinek and Marek Borowiec[a]

Department of Applied Mechanics, Lublin University of Technology, Nadbystrzycka 36, 20-618, Lublin, Poland

Received: 22 April 2015 / Revised: 28 August 2015
Published online: 7 October 2015

Abstract. This paper discusses the problem of stability in a milling process for titanium super-alloy Ti6242. The phenomenon of chatter vibration is analysed by the multiscale entropy method and Hurst exponent. Although this problem is often considered based on stability lobe diagrams, theoretical findings do not always agree with experimental results. First, a stability lobe diagram is created based on parameters determined by impact testing. Next, cutting forces are measured in an experiment where the axial cutting depth is gradually increased. Finally, the obtained experimental signals are investigated with respect to stability using the multiscale entropy method and Hurst exponent.

1 Introduction

The problem of stability in cutting and milling processes, particularly under high speed machining (HSM) conditions, is very important in engineering practice. Instability is caused by chatter phenomena which can be generated by regenerative and frictional mechanisms [1]. The regenerative chatter is one of the most common in the literature. However, Wiercigroch *et al.* [2,3], Lipski *et al.* [4], Rusinek *et al.* [5,6] show that the frictional effect is also important because it can produce the so-called frictional (primary) chatter and can even lead to chaotic vibrations [7,8]. Chatter vibrations generated in cutting operations are undesired because they can deteriorate the surface of a finished product, shorten tool life or even destroy the tool or the work piece. This, combined with the properties of hard, difficult-to-machine materials like titanium alloy, poses serious problems in machining [9–13]. Specific properties of titanium alloys such as high strength and their resistance to heat and corrosion are desirable in the civil and military aviation industry to produce extremely loaded components. Therefore, these alloys are often applied in the production of aircrafts, racing cars, and many other devices.

Given the demand for steadily growing productivity, there is a tendency to increase cutting parameters such as cutting speed and feed rate in manufacturing processes. This, however, can lead to self-excited chatter vibrations generated by a regenerative mechanism. To avoid regenerative chatter, the cutting parameters must be defined properly. To this end, the so-called stability lobe diagrams (SLDs) are created, usually based on modal parameters of the tool-holder system, where a rotational speed and depth of cut determine conditions of stable cutting. An advantage of the SLD technique is that it can predict an unstable region of the cutting parameters prior to machining; however, its correctness depends on the accuracy of the modal test. From another point of view, the cutting process can be controlled online by measuring forces, displacements or accelerations in order to prevent instabilities from occurring in a system. Therefore, some researchers measure acoustic emission during the cutting process to obtain experimental SLDs, *e.g.* in [14]. Others use the recurrence plot (RP) technique [15–17], Hilbert-Huang transform (HHT) [18], flicker-noise spectroscopy [19] and the Hurst exponent [20]. In some cases, however, the dynamics of a system requires the use of a multiscale approach. This is particularly true with complex systems which usually exhibit nonlinear behaviour. For this reason, such systems can be best analysed by the increasingly popular sample entropy method [21–23]. This analysis approach provides a relative level of complexity for measured finite length time signals. The method is widely used in medicine diagnostics [24], for measuring physiologic output signals, particularly blood pressure, heart rate or electrical brain activity [25]. Also, it can be used for detecting early symptoms of cardiac arrhythmias [26]. Apart from the sample entropy method, complex behaviours of mechanical systems can also be analysed by multiscale entropy.

[a] e-mail: m.borowiec@pollub.pl

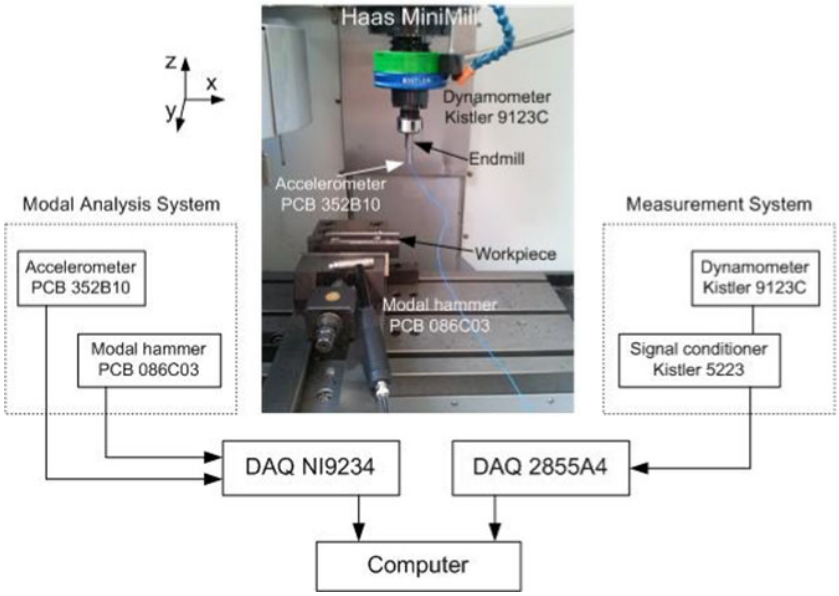

Fig. 1. Scheme of the experimental setup.

The authors of the paper [27] adopted this method to analyse the time series of a bistable laminate plate. They examined its dynamic response, showing the presence of single well and snap-through vibrations of both periodic and chaotic character. The authors of other papers, [15,17], used the multiscale entropy analysis (MSE) to observe fluctuations describing chatter in the milling process of a composite material. This approach was also adopted for time series analysis of vehicle suspension [28,29]. The MSE proved useful in identifying system behaviour during driving tests. This paper uses the composite multiscale entropy analysis ($CMSE$) [30,31] to investigate the milling of the titanium alloy. This method is applied to monitor complex dynamics of machining, particularly with respect to chatter phenomena. Here, the stability of the milling process for titanium alloy Ti6242 is investigated by two approaches: multiscale entropy and Hurst exponent analysis. With these methods, chatter vibrations in machining can be predicted just before they occur.

2 Experiment

The experimental investigations are conducted on a titanium alloy Ti6242 using a Haas MiniMill CNC milling machine. The tests are performed under laboratory conditions at the Łódź University of Technology. Presented schematically in fig. 1, the experimental setup consists of two parts: a modal analysis system (left) and a force measurement system (right). The former, which is used to measure viscoelastic properties of the machine-tool system, consists of a PCB 086C03 modal hammer, a PCB 352B10 accelerometer and an NI9234 data acquisition card (DAQ). The latter is used to measure three components (F_x, F_y and F_z) of the resultant cutting forces and torque (M_z) by means of a Kistler 9123C piezoelectric rotating dynamometer. The dynamometer is connected to a Kistler 5223 signal conditioner and a 2855A4 data acquisition card. Both experimental rigs are integrated in computer system and controlled by the DynoWare software to record measured signals. The measurements are taken in two steps. First, a single point impact test is performed to determine stiffness, natural vibration frequency and damping ratio of the spindle-tool system in order to predict regions of stable milling. To this end, the modal hammer is used to excite the tool and then the output signal is measured by a low mass accelerometer mounted at the tip of the tool. Next, the modal parameters for x and y directions, in the form of frequency response function, are implemented to the CutPro9 software in order to determine SLD analytically. The stability lobe diagram, presented in fig. 2, is generated for the up-milling of titanium alloy Ti6242 by an end milling cutter with a 12 mm diameter and four flutes. The radial depth of cut a_e is set to 4 mm and the feed per tooth f_z is 0.05 mm. Stable cutting occurs in the region below the stability boundary, while unstable machining should occur above the lobes. According to the diagram, the cutting depth below the critical value $a_{pcr} = 1.2$ mm should be stable regardless of the spindle speed.

In order to verify the SLD and find new stability measures, the second part of the experiment is performed using the milling machine. The cutting parameters are set as follows: the spindle rotational speed n is 1860 rpm, the radial depth of cut a_e is 4 mm, the feed per tooth f_z is 0.05 mm, while the axial depth of cut a_p (referred to as "depth of cut") is increased from 0 to 2 mm during the test. The cutting force component F_x and torque M_z are measured and recorded at a sampling rate of 2 kHz, which is the necessary minimum because the natural frequency of spindle-tool

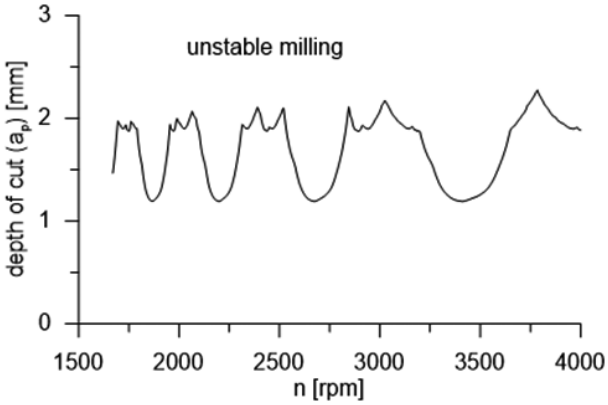

Fig. 2. Stability lobe diagram for up-milling of titanium alloy Ti6242.

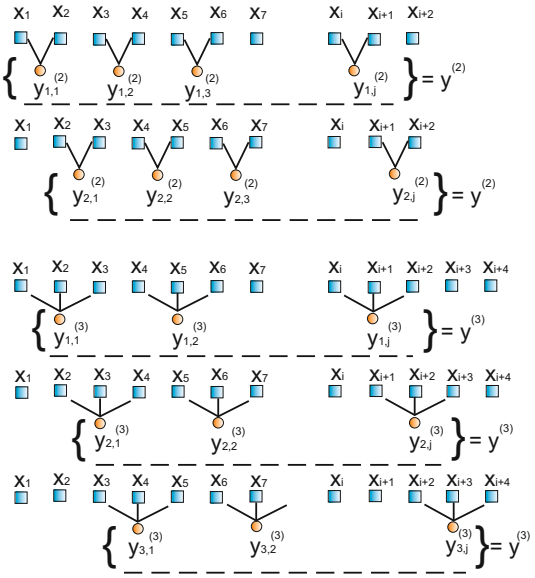

Fig. 3. Schematic representation of a coarse graining procedure for scales $\tau = 2$ and $\tau = 3$.

system amounts to about 800 Hz. The following section contains analyses performed to compare the dynamics of stable and unstable milling systems and to verify whether the theoretical critical depth of cut obtained from the SLD was calculated properly.

3 Multiscale entropy analysis

The composite multi-scale entropy analysis is based on a coarse-graining procedure presented in fig. 3.

This procedure provides a coarse-grained time series as an average of the original data points within non-overlapping windows by increasing the scale factor τ. The k-th coarse-grained time series reads as 1:

$$y_{k,j}^{(\tau)} = \frac{1}{\tau} \sum_{i=(j-1)\tau+k}^{i=j\tau+k-1} x_i, \quad 1 \leqslant j \leqslant N/\tau, \quad 1 \leqslant k \leqslant \tau, \tag{1}$$

where x is a raw one-dimensional time series $x = \{x_1, x_2, \ldots, x_N\}$. For the coarse-grained results $\{y_{k,1}, y_{k,2}, y_{k,3}, \ldots, y_{k,N}\}$, first, two patterns of length $Y_m(i) = \{y_{k,i}, \ldots, y_{i+m}\}$ and $Y_m(j) = \{y_{k,j}, \ldots, y_{j+m}\}$ are selected to compute the number of $Y_m(j)$, which satisfies the condition

$$d[Y_m(i), Y_m(j)] \leqslant r, \tag{2}$$

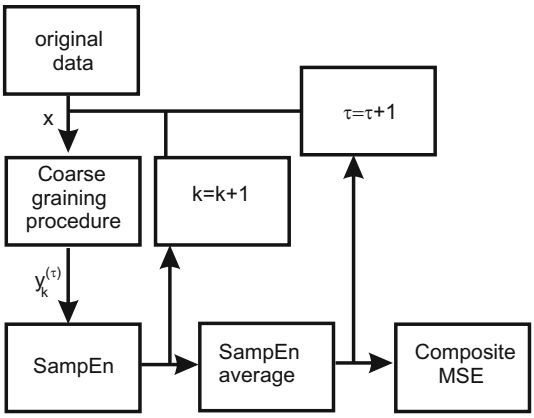

Fig. 4. The algorithm of composite multi-scale entropy.

where $d[Y_m(i), Y_m(j)] = \max[|y_{i+\kappa}, y_{j+\kappa}|](\kappa \in [0, m-1])$ and $j \in [1, N-m]$, $i \neq j$. Finally, the $N_n(i)$ is the result of all $Y_m(i)$ similar to $Y_m(j)$, and the average for $i \in [1, N-m]$,

$$N_n = \frac{1}{N-m} \sum_{i=1}^{N-m} N_n(i) \tag{3}$$

and, next, for the length increase to $m+1$, then

$$N_d = \frac{1}{N-m} \sum_{i=1}^{N-m} N_d(i). \tag{4}$$

The logarithm of the conditional probability that two sequences with a tolerance r are similar to each other at successive points of the coarse-grained series is denoted as $SampEn(\mathbf{y}^{(\tau)}, m, r)$ and defined as [24]

$$SampEn\left(\mathbf{y}_k^{(\tau)}, m, r\right) = \ln\left(\frac{N_n}{N_d}\right). \tag{5}$$

In this approach, for each scale factor τ, the $CMSE$ calculation is based on the time series of the coarse-grained $y_{k,j}^{(\tau)}$ introduced by Wu *et al.* [31]:

$$CMSE(\mathbf{x}, \tau, m, r) = \frac{1}{\tau} \sum_{k=1}^{\tau} SampEn\left(\mathbf{y}_k^{(\tau)}, m, r\right), \tag{6}$$

where $m = 2$ is the pattern length and r is the similarity criterion which is usually chosen to be $r < 0.1\sigma_x$ [32]. Here, σ_x is the standard deviation of the original time series $\{\mathbf{x}\}$.

The algorithm of the composite multi-scale entropy is presented in fig. 4, where the final result for each scale factor τ is the averaged $SampEn$ depending on k-th loops.

The paper investigates real signals reporting a different behaviour of the system characterized by the time series of force and torque signals plotted in figs. 5(a) and (b), respectively. The corresponding magnified extreme parts of these series at the increased depth of cut a_p are presented in figs. 5(c)–(f). The force signal was measured along the feed axis x while the torque was measured on the spindle axle. Generally, it is difficult to observe any differences after the increase in the depth of cut a_p. If one compares the plots of the force signal F_x in figs. 5(c) and (e), and the plots of the torque signal M_z in figs. 5(d) and (f), there is hardly any visible amplitude growth. With long period data, it is recommended using rolling windows to analyse local data. In this paper, the measured signal was first partitioned into a number of windows, and the $CMSE$ was calculated separately for each window data. The window width was taken as 4 and 10 to demonstrate the changeability of signal behaviour.

Figure 6 presents the results of composite multiscale entropy for both the force along the feed axis x and the spindle torque in the z-direction. The results demonstrate that the calculated entropy is higher for the force F_x signal rather than in the case of the torque M_z. This relation remains unchanged at all stage of the cut depth a_p. Analysing the results, one can conclude that the behaviour of the signal along the feed axis of force F_x is more irregular than that of the signal of torque M_z. Additionally, when the milling process is performed at the depth of cut parameter

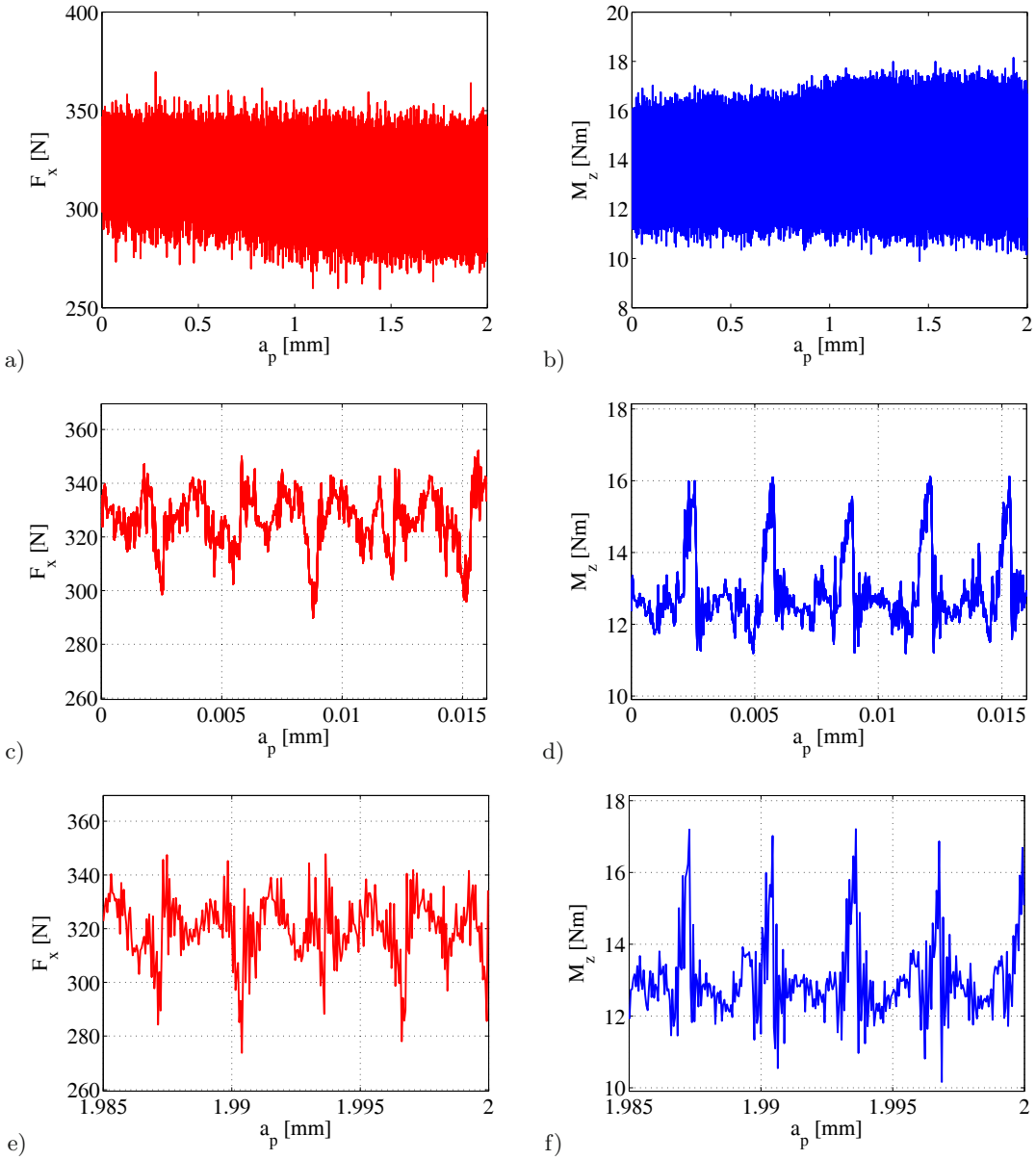

Fig. 5. The time series of the milling process of force signal (a) and torque signal (b). The first part of the wedge data (c), (e) and the final data (d), (f) of force and torque signals, respectively, in Ti6242 alloy milling at increasing the depth of cut a_p, at fixed $n = 1860\,\text{rpm}$, $a_e = 4\,\text{mm}$ and $f_z = 0.05\,\text{mm}$.

$a_p \in (0\text{–}0.5)\,\text{mm}$, this yields the most disordered signals in both measured directions, x and z. By increasing the scale factors τ, the coarse-grained series becomes smoother, and the entropy based on such averaged time series decreases, as expected. Nevertheless, the relation between the signals remains unchanged. In the whole range of τ, the most irregular signal is observed at the smallest value of the a_p parameter, while regularity can be observed at an increased depth of cut ($a_p \approx 2\,\text{mm}$).

Figures 7(a) and (b) show the dependences of $CMSE$ against the depth of cut a_p at chosen scale factors τ. For the smallest $\tau = 1$, the coarse-grained time series is simply the original time series with the highest entropy (red lines). But for all chosen scale factors $\tau = 1$, $\tau = 10$ and $\tau = 20$, the entropy slowly decreases with increasing the a_p parameter.

This means that initiating the milling process at a higher a_p leads to a more regular behaviour of the machining process. This can be clearly observed for the original time series signals ($\tau = 1$, fig. 7). Moreover, in the experiment, the chatter effect is observed at the same values of parameters. Given the results, it can therefore be concluded that the chatter phenomenon in milling manifests itself in a regular behaviour rather than a chaotic one. Finally, the composite multiscale entropy ($CMSE$) maps against both the scale factor τ and the depth of cut a_p are presented in figs. 8(a)

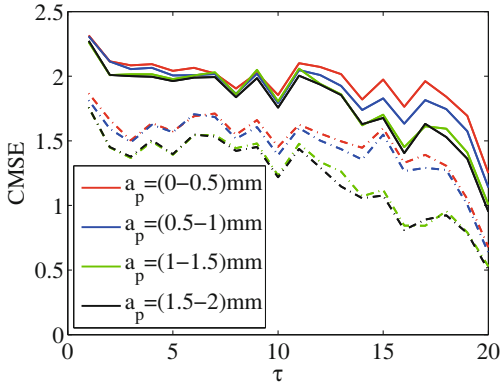

Fig. 6. Composite multiscale entropy $CMSE$ at increasing the depth of cut a_p calculated for force F_x along the feed direction (solid lines) and the $CMSE$ for spindle torque in the z-direction (dashed lines).

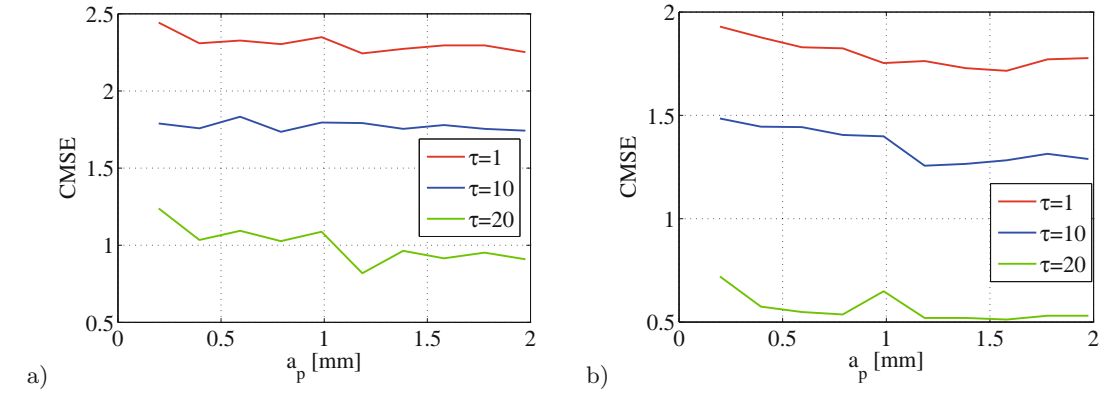

Fig. 7. Composite multiscale entropy against the depth of cut at chosen scale factors τ, for the measured signal of forces F_x (a) and torque M_z signal (b), respectively.

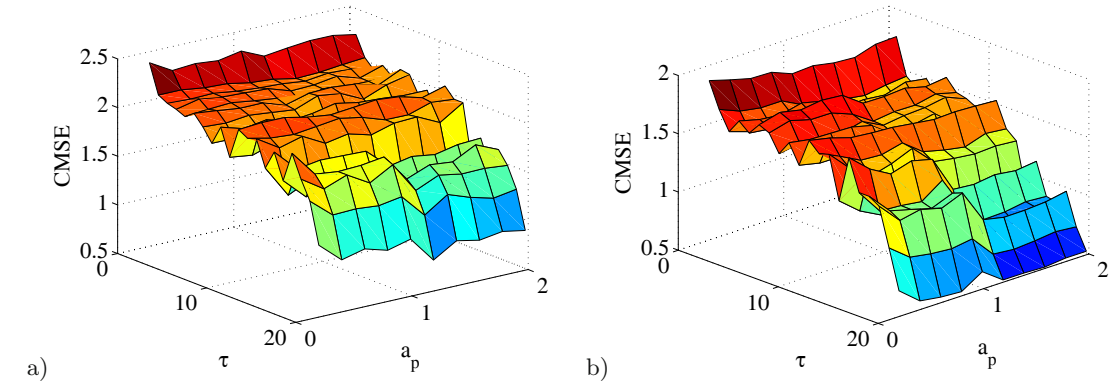

Fig. 8. The maps of composite multiscale entropy against the depth of cut a_p and scale factor τ for measured forces F_x signal (a) and torque signal M_z signal (b), respectively.

and (b). The maps indicate that the system dynamics will remain stable with increasing the depth of cut a_p in the whole range of the scale factor τ. The results reveal the occurrence of chatter.

4 Hurst exponent analysis

Generally, the Hurst exponent is applied to evaluate time series persistence in a long-range dependence. The Hurst exponent can also be interpreted as a measure of the smoothness of a fractal time series based on the asymptotic behaviour of a process. The Hurst exponent is used to solve both in technical [20] and medical [33] problems.

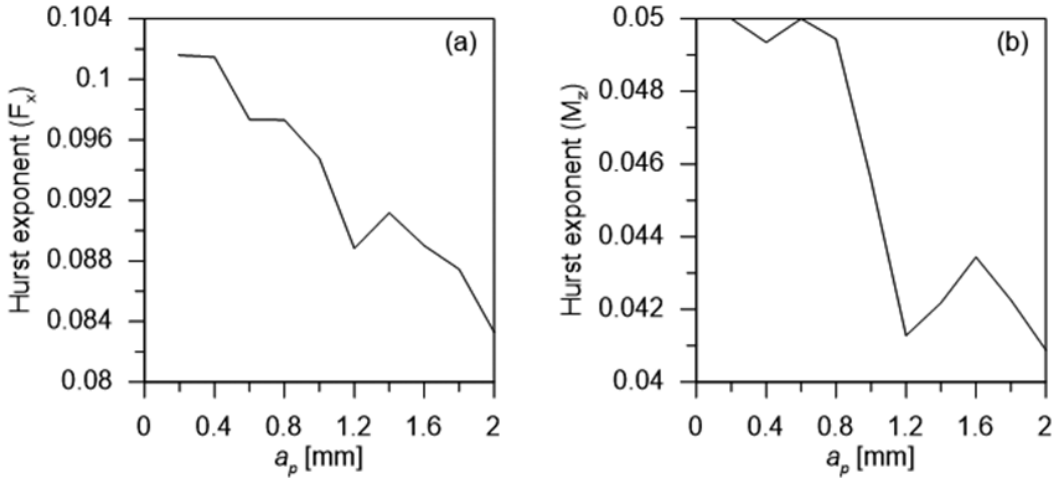

Fig. 9. Hurst exponent of F_x (a) and M_z (b).

The Hurst exponent value ranging between 0 and 0.5 means that the time series demonstrates an "anti-persistent behaviour". This behaviour is sometimes called "mean reversion", which means that future values will have a tendency to return to a longer-term mean value. When the value of the Hurst exponent is between 0.5 and 1 indicating "persistent behaviour", then the time series is trending. If the value is higher than 1, the trend is stronger. Series of this type are easier to predict. The Hurst exponent value close to 0.5 indicates random data (like in a Brownian time series). In this study, the Hurst exponent is used to point out the difference between stable and unstable milling. Both time series (F_x and M_z) exhibit an anti-persistent behaviour. This is connected with changes in signal character which occur during the milling test with increasing the depth of cut. According to the stability lobe diagram in fig. 2, a symptom of stability loss can be observed at the depth of cut $a_p > 1\,\mathrm{mm}$, while the value of the Hurst exponent dramatically decreases (figs. 9(a) and (b)). In general, the Hurst exponent value in the range of 0–0.5 indicates an anti-persistent behaviour of the analysed time series, which confirms that the milling process is susceptible to chatter. Thus, the Hurst exponent can be treated as a relatively good chatter indicator.

5 Conclusions

The composite multiscale entropy ($CMSE$) and Hurst exponent analyses presented in the paper are effective method for detecting chatter. Analysing the stability lobe diagram, one can observe that the unstable behaviour of the milling process at a higher depth of cut a_p, does not provide sufficient information for chatter detection. This stems from the fact that the chatter effect can appear both in chaotic and regular behaviours. As for the analysed time series, the $CMSE$ results reveal a growing disorder at a lower depth of cut a_p, which can indicate some irregularities in the system at the beginning of the process. At the same time, however, it is found that the chatter effect occurs when the depth of cut is increased to $a_p > 1\,\mathrm{mm}$, despite the fact that the behaviour seems regular according to the $CMSE$ analysis. Also, the Hurst exponent analysis confirms that the process can exhibit an anti-persistent behaviour, which can generate this undesired effect. Finally, it can therefore be concluded that unexpected chatter vibrations have regular nature and high amplitude.

Financial support of the Structural Funds in the Innovative Economy Operational Programme (IE OP) financed from the European Regional Development Fund - Project No POIG.0101.02-00-015/08 is gratefully acknowledged.

References

1. M. Wiercigroch, E. Budak, Philos. Trans. R. Soc. Math. Phys. Eng. Sci. **359**, 663 (2001) ISSN 1364-503X.
2. I. Grabec, Phys. Lett. A **117**, 384 (1986).
3. M. Wiercigroch, A.M. Krivtsov, Phil. Trans. R. Soc. London A Math. Phys. Eng. Sci. **359**, 713 (2001).

4. J. Lipski, G. Litak, R. Rusinek, K. Szabelski, A. Teter, J. Warminski, K. Zaleski, J. Sound Vibr. **252**, 739 (2002) ISSN 0022-460X.
5. R. Rusinek, M. Wiercigroch, P. Wahi, Int. J. Mech. Sci. **89**, 167 (2014).
6. R. Rusinek, M. Wiercigroch, P. Wahi, Int. J. Bifurc. Chaos **24**, 1450115 (2014) ISSN 0218-1274.
7. I. Grabec, *Progress in Acoustic Emission III* (The Japanese Society of NDI, 1986) pp. 87–94.
8. I. Grabec, Int. J. Mach. Tools Manuf. **28**, 19 (1998).
9. P.J. Arrazola, A. Garay, L.M. Iriarte, M. Armendia, S. Marya, F. Le Matre, J. Mater. Process. Technol. **209**, 2223 (2009) ISSN 0924-0136.
10. H.W. Hoffmeister, R. Wittmer, C. Schnell, J. Mach. Eng. **9**, 18 (2009).
11. C.H.C. Haron, A. Jawaid, J. Mater. Process. Technol. **166**, 188 (2005) ISSN 0924-0136.
12. S. Al-Zubaidi, J.A. Ghani, C.H.C. Haron, Meccanica **48**, 1701 (2013) ISSN 0025-6455.
13. E.O. Ezugwu, Z.M. Wang, J. Mater. Process. Technol. **68**, 262 (1997) ISSN 0924-0136.
14. Joao A. Duro, Julian A. Padget, Chris R. Bowen, H. Alicia Kim, Aydin Nassehi, Mech. Syst. Signal Process. **66-67**, 505 (2016) DOI: 10.1016/j.ymssp.2015.04.019.
15. G. Litak, A. Syta, R. Rusinek, Int. J. Adv. Manuf. Technol. **56**, 445 (2011) ISSN 0268-3768.
16. R. Rusinek, Proc. Inst. Mech. Eng. B J. Eng. Manuf. **226**, 1976 (2012) ISSN 0954-4054.
17. G. Litak, S. Schubert, G. Radons, Nonlinear Dyn. **69**, 1255 (2012) ISSN 0924-090X.
18. G. Litak, K. Kecik, R. Rusinek, Latin Am. J. Solids Struct. **10**, 133 (2013) ISSN 1679-7825.
19. G. Litak, Y.S. Polyakov, S.F. Timashev, R. Rusinek, Physica A Stat. Mech. Appl. **392**, 6052 (2013) ISSN 0378-4371.
20. K. Kecik, R. Rusinek, J. Warminski, Int. J. Bifurc. Chaos **21**, 1 (2011) ISSN 0218-1274.
21. C.R. Bowen, H.A. Kim, P.M. Weaver, S. Dunn, Energy Environ. Sci. **7**, 25 (2014) ISSN 1754-5692, DOI: 10.1039/C3EE42454E.
22. M. Costa, A. Goldberger, C.K. Peng, Phys. Rev. Lett. **89**, 068102 (2002) DOI: 10.1103/PhysRevLett.89.068102.
23. Y.H. Pan, Y.H. Wang, K.T. Lee, J. Marine Sci. Technol. **19**, 107 (2011).
24. Douglas E. Lake, Joshua S. Richman, M. Pamela Griffin, J. Randall Moorman, Am. J. Physiol. Regul. Integr. Comp. Physiol. **283**, 789 (2002).
25. M.D. Costa, C.K. Peng, A.L. Goldberger, Cardiovasc. Eng. **8**, 88 (2008) DOI: 10.1007/s10558-007-9049-1.
26. R.A. Thuraisingham, G.A. Gottwald, Physica A Stat. Mech. Appl. **366**, 323 (2006) ISSN 03784371.
27. M. Borowiec, A. Rysak, D.N. Betts, C.R. Bowen, H.A. Kim, G. Litak, Eur. Phys. J. Plus **129**, 211 (2014) DOI: 10.1140/epjp/i2014-14211-3.
28. Marek Borowiec, Asok K. Sen, Grzegorz Litak, Jacek Hunicz, Grzegorz Koszaka, Andrzej Niewczas, Forsch. Ing. **74**, 99 (2010).
29. Grzegorz Litak, Marek Borowiec, Jacek Hunicz, Grzegorz Koszaka, Andrzej Niewczas, Chaos Solitons Fractals **42**, 270 (2009).
30. Q. Liu, Q. Wei, S.Z. Fan, C.W. Lu, T.Y. Lin, M.F. Abbod, J.S. Shieh, Entropy **14**, 978 (2012) ISSN 1099-4300.
31. S.D. Wu, C.W. Wu, S.G. Lin, C.C. Wang, K.Y. Lee, Entropy **15**, 1069 (2013) ISSN 1099-4300.
32. M. Costa, C.K. Peng, A. L. Goldberger, J.M. Hausdorff, Physica A Stat. Mech. Appl. **330**, 53 (2003) ISSN 03784371.
33. R. Rusinek, M. Szymanski, J. Warminski, M. Zadrozniak, K. Morshed, Med. Sci. Mon. **17**, 372 (2011).